King Saud University

Arabian Journal of Chemistry

www.ksu.edu.sa
www.sciencedirect.com

ORIGINAL ARTICLE

Facile preparation of micro-porous biochar from Bangladeshi sprouted agricultural waste (corncob) via in-house built heating chamber for cationic dye removal

Nigar Sultana Pinky [a], Mashrafi Bin Mobarak [a,*], Sonjida Mustafi [a],
Mohammad Zesanur Rahman [b], Aynun Nahar [c], Trissa Saha [d],
Newaz Mohammed Bahadur [b]

[a] Institute of Glass and Ceramic Research and Testing (IGCRT), Bangladesh Council of Scientific and Industrial Research (BCSIR), Dhaka 1205, Bangladesh
[b] Department of Applied Chemistry and Chemical Engineering, Noakhali Science and Technology University, Noakhali, Bangladesh
[c] Institute of National Analytical Research and Services (INARS), Bangladesh Council of Scientific and Industrial Research (BCSIR), Dhaka 1205, Bangladesh
[d] Institute of Fuel Research and Development (IFRD), Bangladesh Council of Scientific and Industrial Research (BCSIR), Dhaka 1205, Bangladesh

Abstract Herein, in-house built heating chamber aided facile preparation of biochar was carried out using Bangladeshi sprouted corncob as the precursor for removing methylene blue (MB). The corncob biomass (CCB) was pyrolyzed at 700 °C for 2hrs (heating rate: 10 °C/min) using the in-house built heating chamber in a muffle furnace, eliminating the necessity of pyrolytic chamber. The prepared corncob biochar (CCBC) was characterized for elemental composition, crystallinity (XRD), functional groups (ATR-FTIR), surface morphology-elemental composition (SEM-EDX), surface area (BET), surface charge (point of zero charge), particle size-stability (DLS-zeta potential) and thermal stability (STA). Adsorption efficacy of CCBC was investigated in batch experiment with MB dye as well as effect of various factors such as contact time (5–120 min), initial MB concentration (7–15 mg/L), pH (2–10) and adsorbent dosage (10–35 mg). Without any chemical treatment for activation, CCBC produced maximum adsorption

* Corresponding author.
 E-mail address: mashrafibinmobarak@gmail.com (M. Bin Mobarak).
Peer review under responsibility of King Saud University.

Production and hosting by Elsevier

capacity (Q_{max}) of 20.42mgg^{-1} at 25 °C. The adsorption behavior of MB by CCBC could be better understood by Langmuir isotherm and Pseudo-second order kinetic model as they were the best fitted isotherm and kinetic models. Thus, waste to treat waste, meaning agricultural wastes like corncob can easily be converted into effective adsorbent for treating dye bearing wastewater.

1. Introduction

Dearth of water along with water pollution have been posing an alarming scenario to the scientific community (Hasan et al., 2019; Quispe et al., 2022; Yaseen et al., 2019). "Clean Water and Sanitation", the 6th goal of United Nations Sustainable Development Goals (SDGs), is anticipated to be accomplished by the year 2030. The vexatious unbridled contamination of water sources by anthropogenic sources and growing population are mounting concerns to researchers across the world (Issaka et al., 2022; Palansooriya et al., 2020). One of the most crucial contaminants responsible for polluting water is the dye bearing wastewater (Mishra et al., 2010; Sobhani, 2022). Several industries such as textile, food, furniture and paint etc. use dye as a prime chemical. Textile industries contribute to 20% (approximately) of the total discharged wastewater according to World Bank Report (Keskin et al., 2021; Tavangar et al., 2019). With trivial biodegradability, dyes are carcinogenic and under sunlight its half-life is higher than 2000 hrs (Bessy et al., 2022). However, researchers are struggling worldwide to find the best possible solution that leads to the effective treatment of dye contaminated water (Chan et al., 2011).

According to our literature survey, a number of techniques are in operation for remediation; for instance, adsorption, membrane filtration, coagulation, ion exchange which are attributed to physical treatment whereas photocatalytic degradation, ozonation, fenton reagents, hypochlorite treatment, electrodialysis, chemical precipitation, electrochemical treatments are considered as chemical treatment. The biological treatment method comprises aerobic/anaerobic digestion of dye bearing effluents (Bessy et al., 2022; Keskin et al., 2021; Mobarak et al., 2022; Moosavi et al., 2020; Shakoor et al., 2020; Tavangar et al., 2019). Above mentioned methods have their particular advantages and disadvantages according to their way of interaction. Generally, methods categorized as physical are quite simple, cost effective but some drawbacks of this method are sludge production, low volume of treatment, need further steps like flocculation etc. (Keskin et al., 2021; Moosavi et al., 2020; Ong et al., 2014; Shahmirzadi and Kargari, 2018). On the contrary, chemical methods exhibit effective decolorization, use low cost reagents in treatment, but show agglomeration, low permeability, poor mass transfer and yield unnecessary sludge including toxic substances are some of the drawbacks (Keskin et al., 2021; Ong et al., 2014). In addition, biological processes are slow, complex to manage and require large footmark but this method cannot satisfactorily meet the discharge criteria (Keskin et al., 2021; Moosavi et al., 2020).

Adsorption technique outweighs the above mentioned effluent treatment methods based on economic perspective, raw materials accessibility, operating flexibility, versatility in design, applicability without prior treatment, no generation of unwanted byproducts, abundancy in variety of sources, and adsorbent recovery probability (Barquilha and Braga, 2021; Bonilla-Petriciolet et al., 2017, 2017; Dotto and McKay, 2020; Helfferich, 1985). Such emoluments made materials like activated carbon, silica gel, activated alumina, zeolites etc. to be the most widely used adsorbents even though the rummage for cheapest as well as effective adsorbents are still underway (Foo and Hameed, 2011). Clays, agricultural, industrial and municipal waste derived adsorbents, also conversant as bio-sorbents, are getting much attention due to lower cost as well as exalted efficacy (Bhatnagar and Sillanpää, 2010; P. S. Kumar et al., 2021; Varsha et al., 2022). Based on the ease of availability and sustainability

of the bio-sorbents, biochar has the supremacy according to a myriad number of studies, which also depicted biochar as an ecological adsorbent. In addition to that, biochar also contributes to waste utilization and/or recycling, thus countenancing the zero waste strategy, particularly for countries with sturdy agriculture (De Bhowmick et al., 2019; Gupta et al., 2009; Inyang et al., 2016; Kong et al., 2014; Oluk et al., 2021). With not much surprises, biochar can be prepared from numerous cost-effective biomasses, i.e., rice straw, pine, palm shell, saw dust, sorghum, coca, coconut, seed, weeds, animal manure etc. (Kwapinski et al., 2010; Lonappan et al., 2016; Nanda et al., 2016). Pyrolysis, hydrothermal carbonization, gasification, flash carbonization and torrefaction are some of the most widely known thermochemical preparation procedures of biochar (Bridgwater, 2012; Ng et al., 2017). Among all the aforementioned procedures, pyrolysis which involves thermal decomposition of plant-derived biomass under low oxic or anoxic conditions to produce biochar has become the most used technique (Cha et al., 2016; Kloss et al., 2012; Sohi et al., 2009).

Biochar is known for its carbon rich porous structure that can be produced by conjunction of thermal treatment and limiting oxygen (Saini et al., 2020; Yang et al., 2015). Physico-chemical properties of biochar such as large surface area and high porosity are said to be exclusive since biochar's adsorption efficacy is directly proportional to these properties (Gayathri et al., 2021; Hemavathy et al., 2020; Yaashikaa et al., 2020). Therefore, fine-tuning of raw materials composition and pyrolysis condition (temperature, rate of reaction, heating time etc.) not only influences the dye removal efficiency but also imparts versatility to biochar for treating a wide range of pollutants (Rafiq et al., 2016). Moreover, treatment with acid, alkali or oxidizing agents significantly improves the properties of biochar (Jothirani et al., 2016; Kumar et al., 2011; Suganya et al., 2017).

Agricultural waste, i.e., corncob biomass becomes a burden when agriculture dependent developing countries like Bangladesh produces 5,400 Kilotons of maize in the fiscal year 2019–2020. Heterogenous micropore structure, high carbon content as well as hemicellulose content etc. are the perquisite of corncob derived biochar which eases the adsorptive removal of azo dyes, MB for instance (Mullen et al., 2010; Suwunwong et al., 2020).

This study of ours utilized locally available corncob waste for preparing biochar using a simplistic inhouse built pyrolysis chamber. The efficacy of the CCBC for adsorptive removal of MB was also evaluated and the kinetic and isotherm data were exploited for finding the best fitted mechanism of adsorption.

2. Materials and methods

2.1. Materials

The precursor biomass (corncob) for biochar preparation was procured from a local market in Dhaka, Bangladesh (Mohammadpur krishi market; 23°45′57.2″N 90°21′33.5″E). Hydrochloric acid (HCl) and ethanol (C$_2$H$_5$OH) were procured from Sigma-Aldrich, UK. Methylene blue, the model dye for the adsorption study was purchased from Merck, Germany with the properties listed in Table 1. Mili-Q water was used at all stages of sample preparation.

Table 1 Properties of methylene blue dye (Al-Qodah et al., 2007).

| Name of the dye	Methylene Blue
IUPAC name	3,7-bis(dimethylamino)-phenothiazin-5-ium chloride
Chemical formula	$C_{16}H_{18}ClN_3S$
Type	Cationic
Molecular weight	373.9 $gmol^{-1}$
Maximum Adsorption Wavelength (λ_{max})	664 nm
Solubility in water	40 g/L
CAS number	61–73-4
Color Index	51
Chemical structure	

2.2. Methods

2.2.1. Preparation of biochar

The preparation of CCBC from CCB has been visualized in Fig. 1a. Briefly, the collected corncobs were washed to remove dirt and loose particles, followed by drying under sunlight for 2–3 days and oven drying for few hours. The dried corncobs were chopped into smaller pieces, grinded in a tumbler ball mill (Pascall Engineering, UK) at 50 rpm and then screened in a 50-mesh sieve to get uniform size. The sieved corncob powder was oven dried at 105 °C and stored in an airtight container. Requisite amount of CCB powder was first taken in a ceramic crucible with a lid, placed in an in-house built stainless-steel chamber (Fig. 1b) of length × width × height: 12″ × 12″ × 7″ (Fig. 1c) and subjected to pyrolysis at 700 °C for 2 h in a Muffle furnace (Nabertherm L3/11/C6, Germany). The rate of heating was maintained at 10 °C per min. After completion of pyrolysis, the prepared biochar was washed with distilled water in order to neutralize the pH. Washing with HCl ($1 molL^{-1}$) and absolute ethanol were also done to remove residual ash and organic impurities. After washing, the biochar powder was oven dried and stored in airtight conditions.

2.2.2. Adsorption experiments

The adsorption experiment involved taking 30 ml of MB dye in 100 ml Erlenmeyer flasks, placing it in an orbital shaker and shaking at 150 rpm under ambient conditions. Different concentrations of MB solution were prepared by diluting the stock solution (1000 ppm MB) as required. Effect of different factors, i.e., pH (2–10), contact time (5–120 min), initial dye concentration (7–15 mg/L) and adsorbent dosage (0.010–0.035g) were also studied. pH adjustments were done with HCl and NaOH solutions (0.1 M each). The adsorbent was separated by centrifugation at 6000 rpm shortly after completion of orbital shaking. Absorbance of the separated solution was
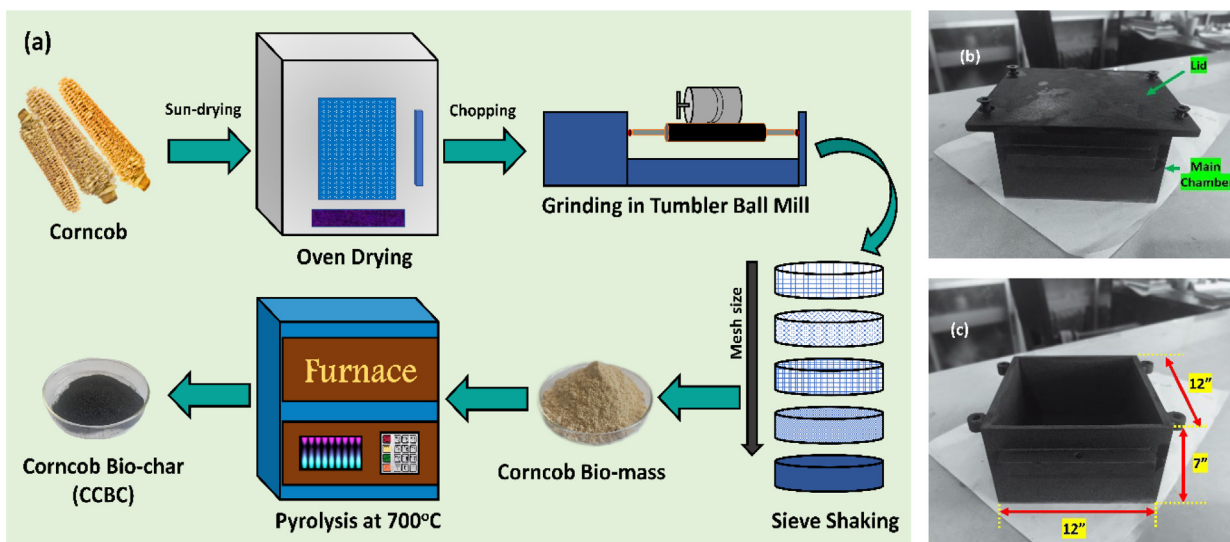
Fig. 1 (a) Preparation scheme of bio-char from corncob; (b and c) in-house built heating chamber.

recorded using a UV–Vis spectrophotometer (Shimadzu UV-1800) at 664 nm. The kinetics and isothermal study of the MB adsorption onto CCBC were also done varying the contact time and initial MB concentration respectively. The adsorption of MB onto CCBC at time t, q_t (mg/g), at equilibrium q_e (mg/g) and removal percentage was calculated by the following equations (1) to (3) (Ganguly et al., 2020),

$$q_t = \frac{C_0 - C_t}{W} \times V \tag{1}$$

$$q_e = \frac{C_0 - C_e}{W} \times V \tag{2}$$

$$Removal Percentage = \frac{C_0 - C_t}{C_0} \times 100 \tag{3}$$

where C_o, C_t and C_e = initial, at time t and equilibrium concentration (mg/L) of MB solution; W = adsorbent dose (g) and V = volume of MB (L).

3. Characterization

The elements of CCBC; more specifically C, H, N, S and O were quantified by an elemental analyzer (Vario EL Cube, Elementar, Germany). Phase analysis was carried out by X-ray powder diffractometer (Rigaku Smart Lab). The XRD analysis was done within the 2θ range of 10° to 80° and the X-Rays were generated using ceramic made Cu tube (CuKα radiation with λ = 1.54060 Å). Other operating conditions were: fixing step = 0.01°, scanning rate = 30°/min, voltage = 40 kV and current = 50 mA).

The presence of functional groups in CCBC were identified with ATR-FTIR (Attenuated Total Reflectance-Fourier Transform Infrared Spectroscopy) instrument (Shimadzu IR Prestige-21 with MIRacle-10 ATR accessory). Surface structure of CCBC was explored by Scanning Electron Microscope (Phenom Pro-Desktop 1481). The elemental analysis of CCBC was carried out with Energy Dispersive X-ray spectroscopy (TEAM EDS; EDAX, USA).

Particle size as well as zeta potential were determined by a DLS instrument (Malvern Panalytical Zetasizer Ultra). The power and wavelength of the equipped laser were 10mW and 632.8 nm respectively. The CCBC sample was finely dispersed in Mili-Q water and sonicated for 15 min before DLS analysis. The nitrogen adsorption–desorption isotherm was measured using Brunauer-Emmett-Teller (BET) sorptometer (BET-201-A, PMI, Tampa, FL, USA). Prior to the BET analysis, the sample was degassed at 120 °C for 9 h.

TGA (thermogravimetric analysis) and DSC (differential scanning calorimetry) analysis were carried out for thermal stability profiling of the prepared CCBC adsorbent by the aid of a simultaneous thermal analyzer (STA) (NETZSCH STA 449F5). The point of zero charge (pH$_{PZC}$) of CCBC was determined adapting the pH drift method with little alteration which is also reported by other literatures (Barquilha et al., 2019; Giri et al., 2020; Pohanish, 2017). In 100 ml conical flasks, 0.02 g CCBC and 50 ml 0.1 M NaCl solution was added and placed for orbital shaking at 150 rpm for 12 h at 25 °C. The pH of NaCl solution was maintained 3–12 by using NaOH and HCl solution. The initial and final value of pH is measured using pH meter. pH$_{PZC}$ was calculated by plotting the change

in pH (ΔpH) against the initial pH of the samples (Sumalinog et al., 2018). The equation (4) for ΔpH is as follows:

$$\Delta pH = pH_{final} - pH_{initial} \tag{4}$$

4. Results and discussion

4.1. Elemental analysis

Elemental composition (C, H, N, S and O) together with different molecular ratios H/C, O/C and (O + N)/C of native sprouted CCB and CCBC were analyzed and represented in Tables 2 and 3 respectively. The obtained values of elemental composition of CCB were compared with CCB from different regions of the world. CCB used in our study showed difference in percentage of carbon and oxygen compared to the consistent values from other regions.

Elemental analysis of CCB gives insight of several characteristics such as polarity index, hydrophilicity and aromaticity. This helps to assess the potentiality of biochar for intended application. According to Table 2, the CCB used in all the studies contain low percentage of nitrogen and sulfur which signifies environment friendly feedstock with low rates of nitrogen oxide and sulphur oxide emission during pyrolysis (Mohamed Noor et al., 2012).

The elemental compositions (C, H, O, N; O/C, H/C and (O + N)/C ratio) of CCB (Table 2) have decreased after pyrolysis at high temperature (Table 3) which is due to their elimination as H_2O, CO_2, and CO molecules during pyrolysis (Worasuwannarak et al., 2007). Percentage of carbon in CCBC rose substantially from 41.01% to 78.05% where possible reason could be the removal of –OH groups during dehydration (Gupta et al., 2018). In addition, Cracking of nitrile group, NO_x, NH_3 during high temperature pyrolysis attributed for the decrease of N content (Tian et al., 2013). The decrease in H/C, O/C and (O + N)/C ratios in CCBC depicts complete carbonation, good aromatization, better aromaticity and stability, lower hydrophilicity and polar functional groups on the biochar surface (Dieguez-Alonso et al., 2018; Hao et al., 2013; Stefaniuk and Oleszczuk, 2015). Life span of biochar is also a crucial parameter to predict based on O/C ratio. According to Spokas K.A., when the O/C ratio is between the value of 0.2 to 0.6, it is predicted to have a life span of 100 years (Anupam et al., 2015; Spokas, 2010). Our prepared CCBC has O/C ratio of 0.23, which depicts its 100 years life span.

4.2. X-ray powder diffraction study

The XRD diffractogram of CCBC sample pyrolyzed at 700 °C is shown in the Fig. 2. The pattern shows two broad humps like diffraction peaks within the 2θ angle of 17.42°~27.72° and 38.12°~46.71°.

This substantify the formation of amorphous phase of the biochar which begets due to the disorderly stacked up carbon rings. These two broad peaks correspond to (0 0 2) and (0 0 1) plane of amorphous form of carbon (Gonzalez-Canche et al., 2021; Saremi et al., 2020; Villagómez-Salas et al., 2018; Yeboah et al., 2020). According to Mreohan et. al. (Mohan et al., 2018), the existence of (0 0 2) plane might be due to the

Table 2 Comparison of elemental composition of corncob biomass from different region.

Elements	Bangladeshi sprouted (wt%)	Middle eastern part of China (wt%)	Serbian (wt%)	Hawaiian (wt%)	Turkish Marmara regional (wt%)	Turkish East Black Sea regional (wt%)
C	41.01	48.12	47.6	47.0	49.32	49.0
H	6.66	6.48	6.3	6.4	5.35	5.6
N	1.71	1.89	0.6	0.5	0.63	0.5
S	–	–	0.2	0.1	–	–
O*	50.62	43.51	43.9	43.4	44.70	43.8
H/C	0.16	0.13	0.13	0.13	1.52	0.11
O/C	1.23	0.90	0.92	0.92	0.9	0.89
(O + N)/C	1.27	0.94	0.93	0.93	0.91	0.90
Ref.	This study	(Liu et al., 2014)	(Trninić et al., 2012)		(Demiral et al., 2012)	(Demirbas, 2004)

*Oxygen value = 100 - (% carbon + % hydrogen + % nitrogen + % sulfur) (Ro et al., 2010).

Table 3 Elemental composition of CCBC.

| Elements	Percentage (%)
C	78.05
H	2.21
N	1.26
S	–
O	18.48
H/C	0.028
O/C	0.23
(O + N)/C	0.25
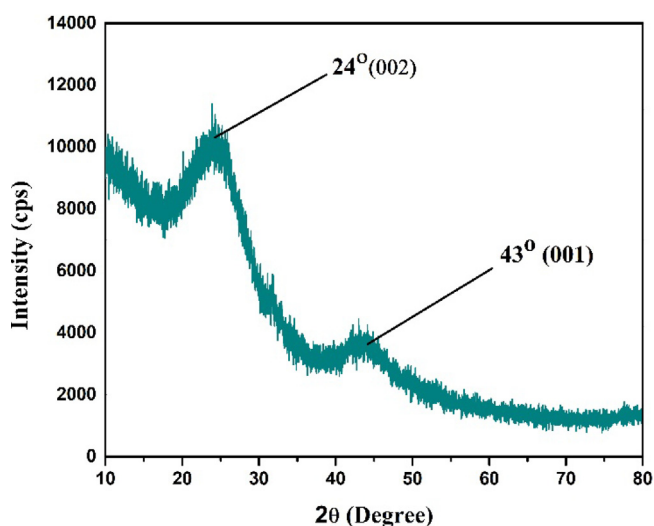
Fig. 2 XRD pattern of the prepared CCBC.

parallel and azimuthal orientation of the aromatic, partially carbonized lamellae (Zhang et al., 2019) whereas the (0 0 1) plane might be due to the condensed aromatic carbonized planes (Wang et al., 2022). Nevertheless, absence of any sharp peaks alluded no crystallinity which might have happened due to the presence of silica or relevant other inorganic metal oxide impurities (Mohan et al., 2018; Petronijević et al., 2021).

4.3. ATR-FTIR study

Fig. 3 exhibits the ATR-FTIR spectra of CCB, CCBC and MB dye loaded CCBC for characterization based on functional groups. For the CCB (Fig. 3a), the –OH stretching vibration was observed at the broad absorption peak of 3334 cm^{-1} (Chakraborty et al., 2018; Zhao et al., 2021). The C–H stretching vibrational peak at 2883 cm^{-1} might be from the hemicellulose and cellulose structure (N. S. Kumar et al., 2021; Wang et al., 2019). The band at 1637 cm^{-1} can be assigned to the aromatic C = C bond while band at 1382 cm^{-1} can assigned to the N-O symmetric nitro group (Chen et al., 2012; N. S. Kumar et al., 2021). In addition, a series of peaks at 1000 ∼ 1305 cm^{-1} can be assigned to assorted functional groups with oxygen (Chen et al., 2012).

At elevated pyrolysis temperature (700 °C), most major bands of CCB disappeared while converting into CCBC due to the degree of carbonization. In case of CCBC, aromatic C–H deformation at 700 cm^{-1} with increased intensities is also observed compared to pristine biomass (Wang et al., 2018). The bands at around 1520 cm^{-1} (Fig. 3 a, b and c) represent aromatic ring vibrations from lignin structure. The intensity
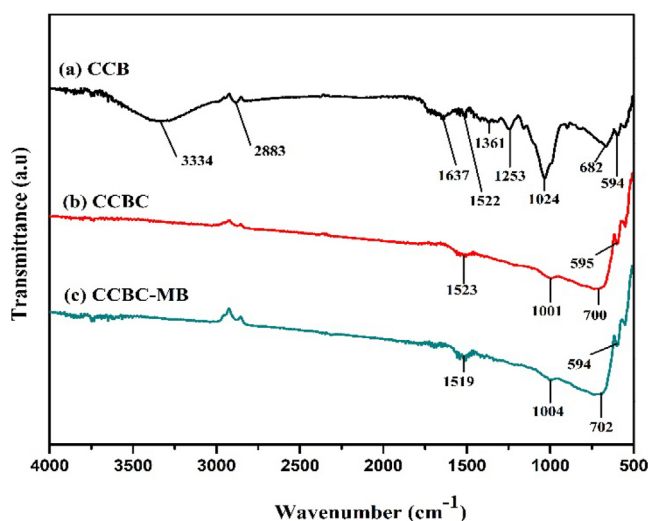
Fig. 3 ATR-FTIR spectra of (a) CCB, (b) CCBC and (c) CCBC-MB.

of the band at 1024 cm^{-1} got decreased after pyrolysis which corresponds to the C–O–C stretching vibration (Fig. 3 a and b). The bands below 1000 cm^{-1} are related to hydroxyl and cellulose groups (Wang et al., 2019). The MB dye loaded CCBC shows almost identical spectrum as CCBC, except for few changes in peak positions. This predicts higher cycles of reusability from the prepared CCBC.

4.4. SEM and EDX study

The surface morphology and micro-structure of biochar was investigated by SEM analysis (Fig. 4). From Fig. 4a, the presence of varied size of granules and pores distribution throughout the entire surface was quite visible and this provided more active sites to bind with dye molecules at various magnitudes (Ma et al., 2021).

The existence of rough spongy surface was also confirmed by SEM analysis. This structural phenomena is the result of formation of porous channel due to the elimination of volatile organic materials as well as demolition of fiber structure at elevated temperature while pyrolysis was carried out (N. S. Kumar et al., 2021; Wu et al., 2020). The EDX spectrum of CCBC is shown in Fig. 4d. Three main constituents, i.e., C, N and O were detected through the EDX analysis where C, N and O were 85.83%, 3.76% and 10.40% respectively. Higher carbon content as well as low oxygen content substantify the effectiveness of the in-house built pyrolytic chamber (Adesemuyi et al., 2020).

4.5. Point of zero charge

The surface charge of the adsorbent becomes zero at a specific pH value and this value is termed as point of zero charge (pH$_{pzc}$) (Nath et al., 2021). This parameter is important for understanding the mechanism and optimum conditions for adsorptive removal of pollutants like dyes or heavy metals. Fig. 5 shows the pH$_{pzc}$ of the prepared CCBC adsorbent.

From the plot of ΔpH vs the initial pH, the intersection point along the x-axis represents the pH$_{PZC}$ (Gatabi et al., 2016). According to such, the pH$_{PZC}$ of CCBC was 6.8 which means the net surface charge of CCBC becomes zero at pH 6.8 (Cruz et al., 2020). When the value of pH < pH$_{pzc}$, it indicates the surface of CCBC is positive and can easily interact with anionic dyes whereas pH > pH$_{pzc}$ denotes the negatively charged surface of CCBC and its preferable reaction with cationic dyes (El Haddad et al., 2012). Thus, maintaining pH of solution above 6.8 will favor the removal of cationic dyes like MB. Effect of pH in batch experiment also supports the statement as highest MB removal was seen at pH 8, which is higher than the pH$_{PZC}$ (6.8).

4.6. BET analysis

The BET analysis was carried out to determine the surface area (S$_{BET}$) and pore size distribution of CCBC based on N$_2$ adsorption/desorption isotherms at − 196 °C which is presented in Fig. 6 (a and b). S$_{BET}$ of CCBC adsorbent was found

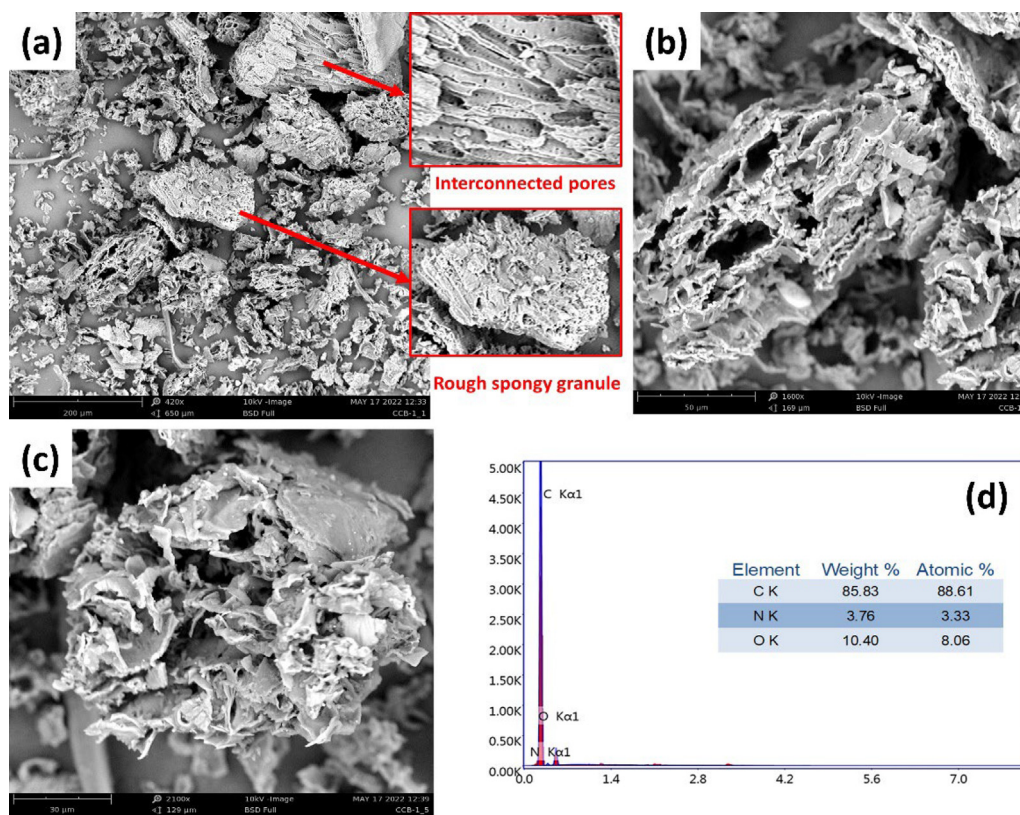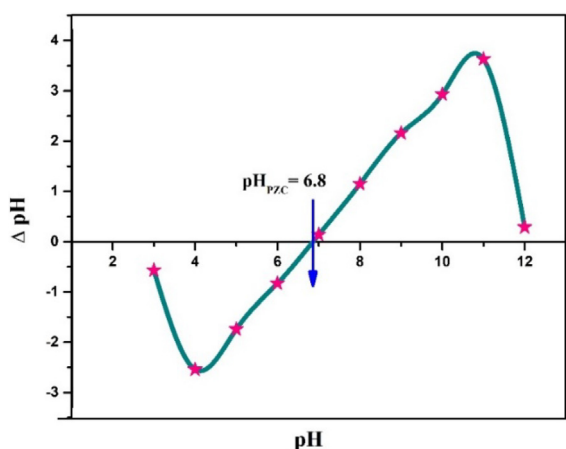**Fig. 4**   (a-c) SEM images and (d) EDX spectrum with elemental composition of CCBC.

Fig. 5 Plot of pH_{PZC} determination of CCBC.

to be 435.15 m^2/g. Such a large surface area might be due to the fact that, at elevated pyrolytic temperature, the volatile components present in the adsorbent get eliminated creating tiniest of interconnecting pores (Vyavahare et al., 2021). Then again, the micropore surface area was found 394.73 m^2/g (t plot) which is 90% of total surface area. In addition, the shape and a substantial increase in the adsorption volume at the first measurement point of CCBC isotherm also indicates that CCBC is strongly microporous (Maziarka et al., 2021).

According to IUPAC classification, CCBC demonstrates type-I adsorption isotherm curve which depicts the microporous structure of the adsorbent. The H$_4$ type hysteresis loop is also present since non-limiting adsorption is observed at higher relative pressure. This also implies the uniform narrow slit-shaped porosity of CCBC. In addition, the pore diameter is 25.33 Å along with 0.2533 cm^3/g total pore volume of the prepared CCBC (N. S. Kumar et al., 2021).

4.7. Particle size and zeta potential analysis

Multi Angle-DLS (MADLS) aided particle size analysis technique was employed for determining the particle size of CCBC.

An average particle size of 432 nm was found and this distribution is shown in Fig. 7a. The consolidated effect of ball milling and sieving of the CCB contributed to such minute sized CCBC particles. The stability of CCBC was measured in terms of zeta potential analysis (Fig. 7b). According to the data obtained, multiple peaks were obtained which corresponded to the values −34.80, −22.12 and −12.43 mV at solution pH. The apex at −22.12 mV as well as the sharp peak at −34.80 mV depict the moderate to good stability of the CCBC particles. The occurrence of such multiple peaks might be due to the significant distribution of particle size of the prepared CCBC adsorbent (Hossain et al., 2020; Wang et al., 2021).

4.8. Thermal analysis

The TGA and DTG (derivative thermogravimetry) profiles of the CCBC (Fig. 8a) show evidences of minute mass change of the prepared CCBC adsorbent which was 4.51% within room temperature to 800 °C. A huge residual mass, quantitatively more than 95% depicts the strong thermal stability of the CCBC particles compared to the CCB (raw material) without compromising its porosity (Zhao et al., 2017).

The TGA curve reveals a dual mass loss step where the first step accounts for 4.49% of mass loss up to 130 °C that is due to the elimination of moisture and volatile organic compounds (Ghodke et al., 2021). The second mass loss was observed after 510 °C up to 800 °C which is attributed to 3.97% weight loss probably due to the elimination of large complex molecules along with inorganic compounds during heat treatment. DTG curve supports the two step wight loss of CCBC. Thus, the amount of residual biochar at 800 °C is 95.49% which depicts strong thermal stability of CCBC (Subratti et al., 2021). The DSC and DDSC (derivative differential scanning calorimetry) curve of CCBC is shown in Fig. 8b. According to the thermogram, two endothermic as well as two exothermic processes were recorded. Peak temperature and the area of the two endothermic processes were 512 °C, +89.93 J/g and 605.9 °C, +80.95 J/g respectively whereas peak temperature and area of 73.7 °C, −7.905 J/g and 154.3 °C, −94.84 J/g respectively were observed for the two exothermic processes.
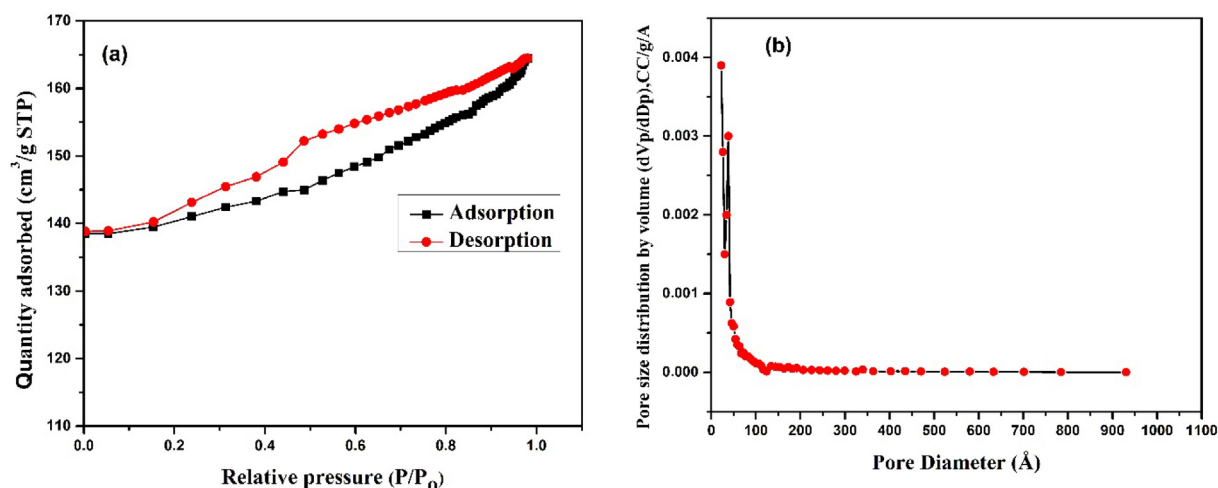

Fig. 6 BET analysis of CCBC (a) N$_2$ adsorption–desorption isotherm, (b) BJH adsorption pore size distribution curve.
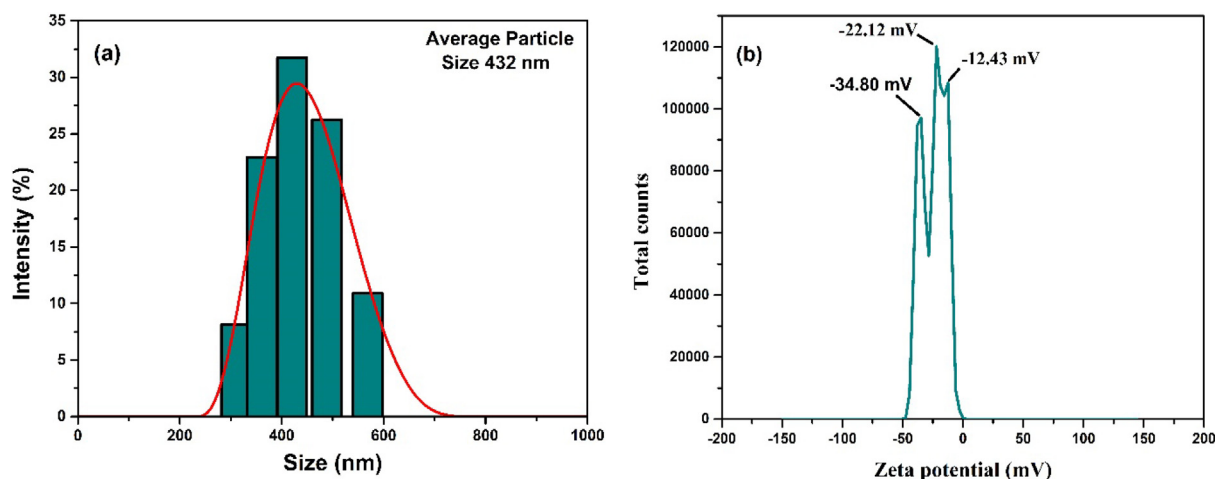
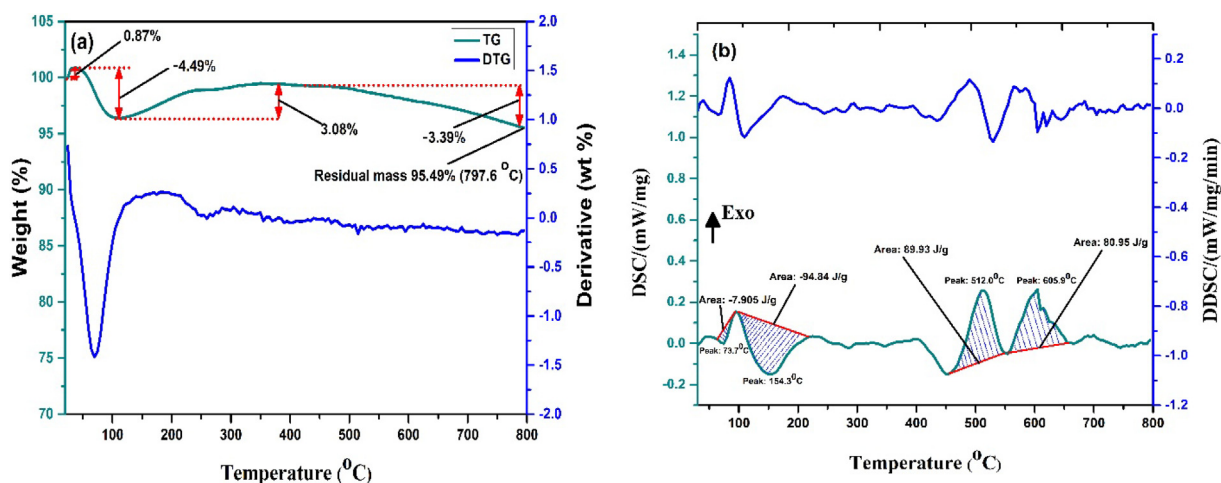**Fig. 7** (a) DLS particle size and (b) zeta potential (at solution pH) analysis of CCBC.

Fig. 8 (a)TGA -DTG and (b) DSC-DDSC curve of prepared CCBC sample pyrolyzed at 700 °C.

4.9. Adsorption studies

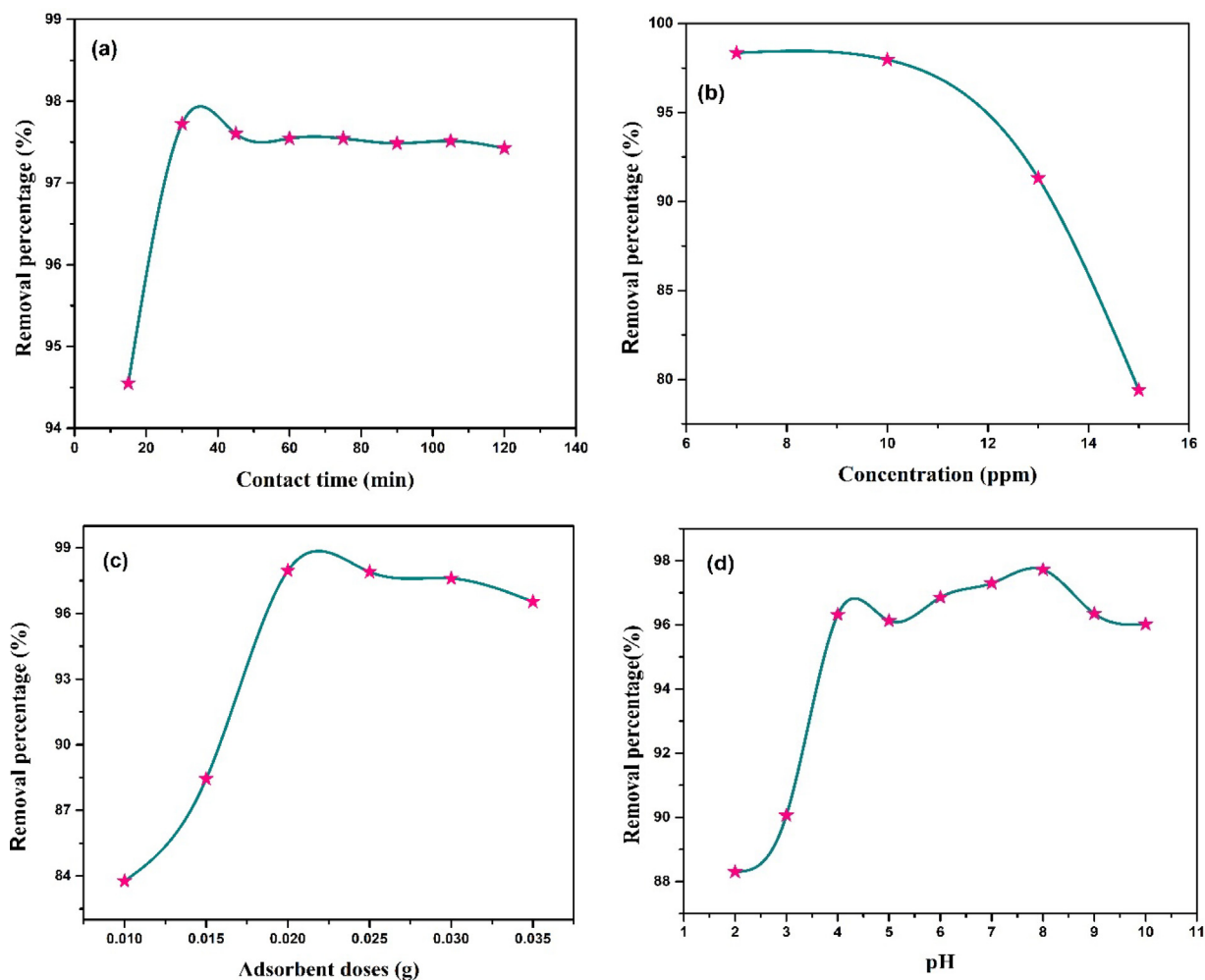#### 4.9.1. Effect of contact time and initial MB concentration

Cost effectiveness as well as economic benefits are greatly influenced by the contact time during any treatment process. Herein, the effect of contact time and initial MB concentration on removal percentage was experimented with various shaking durations ranging from 5 to 120 min and MB concentration from 7 to 15 ppm. The results have been shown in Fig. 9a and 9b, from which it is clearly understandable that adsorption efficacy of CCBC is dependent on contact time and initial MB concentration. Within 15 min of shaking, around 94% MB removal was attained. Such high percentage of removal within shortest time period was possible because of higher availability of active sites. Only 3% removal was attained in the next 15 min and steady removal was observed for further contact time until equilibrium was achieved after 120 min. Saturation of CCBC surface with MB caused such phenomena since it becomes hard for MB molecules to further find more available sites for adsorption (Adeogun et al., 2018).

4.9.2. Effect of adsorbent dose

The effect of adsorbent dosage on the removal % of MB is shown in Fig. 9c. With the increase of adsorbent dosage from 0.01 g to 0.02 g, the % removal also increases from 83% to 97%. Further increase of CCBC dose doesn't quite increase the removal efficacy and ultimately reached equilibrium for 0.02 g with removal efficiency of 97.72%. This is due to the fact that, at first there were more available active sites for MB to get adsorbed onto CCBC surface. But after equilibrium is achieved, lesser number of active sites are present which caused lower removal rate. In addition, if doses are given in excess amount, there is a chance of adsorbent particle aggregation which will lead to limited binding sites (Shirmardi et al., 2016; Zhu et al., 2018).

4.9.3. Effect of pH

Generally, interaction between adsorbent and adsorbate greatly depends on the solution pH (Abd El-Rahim et al., 2009). Fig. 9d represents the relation between % removal and pH of the MB solution (pH ranging from 2 to 10). With the increase of pH from 2 to further, removal percentage also

Fig. 9 (a) Effect of contact time (C_o = 10 ppm, CCBC dose = 0.02 g, pH = 8, shaking speed = 100 rpm); (b) Effect of initial MB concentration (CCBC dose = 0.02 g, pH = natural, shaking speed and time = 100 rpm and 30 min); (c) Effect of adsorbent dose (C_o = 10 ppm, pH = natural, shaking speed and time = 100 rpm and 30 min) and (d) Effect of pH for MB adsorption on CCBC (C_o = 10 ppm, CCBC dose = 0.02 g, shaking speed and time = 100 rpm and 30 min); all the experiments were carried out at 25 °C.

rose sharply till pH 4 and then remained almost steady up to pH 6. Maximum removal percentage was attained at pH 8 (97.7%) and further increase in pH led the removal percentage drop to 96% (pH 10). Nath et. al. also reported similar results where maximum MB was adsorbed at pH 8 on okra (*Abelmoschus esculentus L.*) mucilage modified biochar (Nath et al., 2021). At lower pH, the concentration of H$^+$ ions are high as well as various surface-active sites become protonated which renders biochar surface with positive ions. This leads to the electric repulsion between cationic MB and CCBC. On the contrary, at increased pH, deprotonation of active sites made the CCBC surface negatively charged which facilitated the electrostatic attraction between CCBC surface and MB molecules. The saturation of adsorbent with cationic MB molecules can be clearly observed by steady portion of the fig at pH 5–6 (Nath et al., 2021).

4.10. Adsorption isotherms

In adsorption processes at equilibrium, isotherm models play significant role in providing information about the adsorption

efficiency, favorability, mechanism and affinity between adsorbate and adsorbent (Kyzas and Matis, 2015; Wang et al., 2018). For the adsorption of MB onto CCBC surface, different isothermal models such as Langmuir, Freundlich, Temkin and Dubinin–Radushkevich (D–R) were employed for analyzing the equilibrium data. The linear forms of Langmuir and Freundlich isotherm models are presented by the equation (5) and (6) whereas their non-linear forms are represented in equation (7) and (8) respectively. The Temkin and D-R isotherm models are represented in equation (9) and (10) respectively (Dubinin, 1947; Freundlich, 1906; Langmuir, 1918; Padmavathy et al., 2016; Temkin, 1940).

$$\frac{Ce}{q_e} = \frac{C_e}{q_m} + \frac{1}{K_L q_m} \tag{5}$$

$$ln q_e = ln K_F + \frac{1}{n} ln C_e \tag{6}$$

$$q_e = \frac{q_m K_L C_e}{1 + K_L C_e} \tag{7}$$

$$q_e = K_F(C_e)^{\frac{1}{n}} \qquad (8)$$

$$q_e = \frac{RT}{b} \ln K_T + \frac{RT}{b} \ln C_e \qquad (9)$$

$$\ln q_e = \ln Q_m - K_E \varepsilon_P^2 \qquad (10)$$

Here, C_e = MB concentration at equilibrium (mgL^{-1}); q_e = amount adsorbed at equilibrium (mgg^{-1}), q_m = maximum adsorption capacity of CCBC (mgg^{-1}); K_L = Langmuir con-
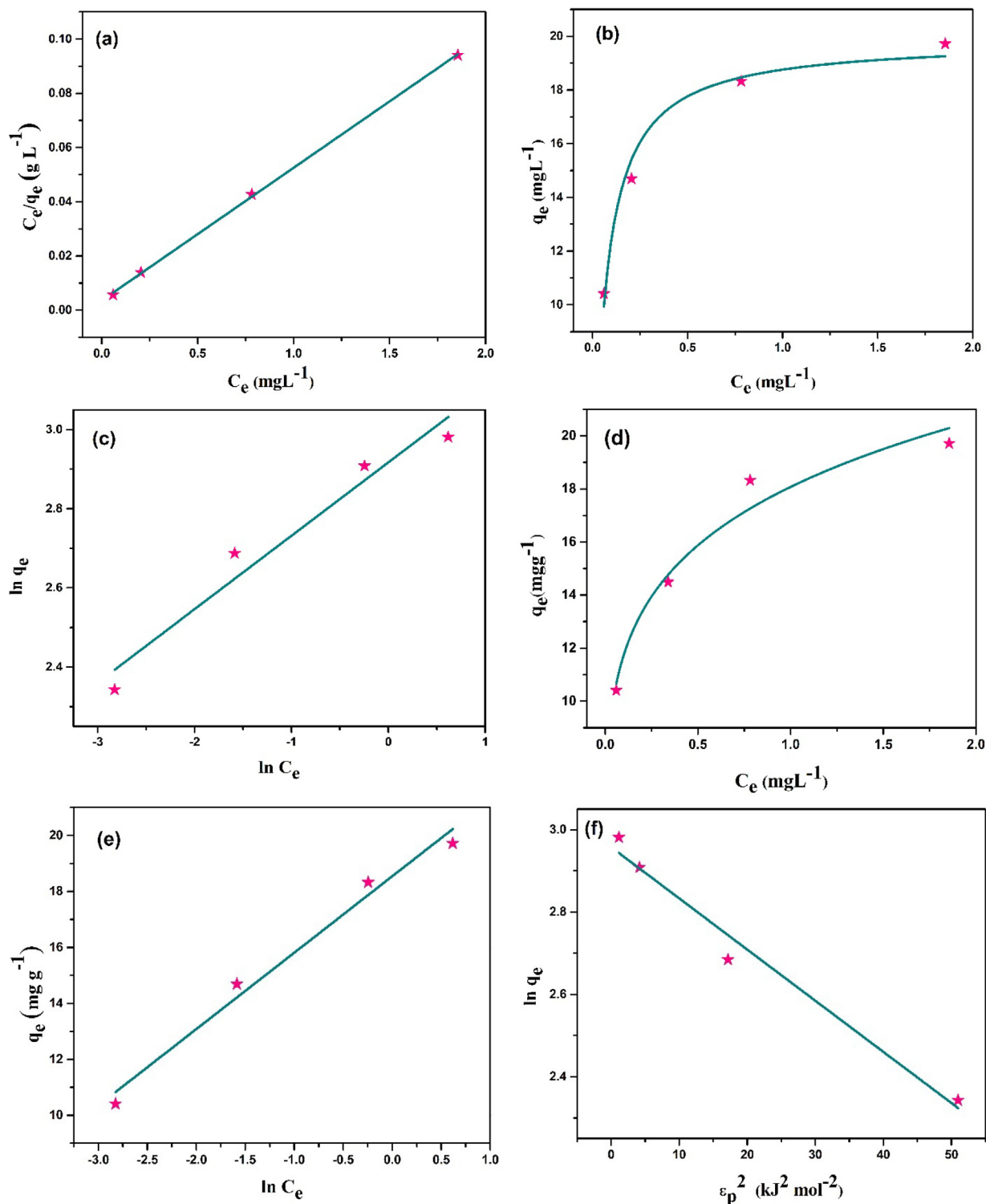
Fig. 10 (a and b) Linear and non-linear form of Langmuir isotherm model; (c and d) linear and non-linear form of Freundlich isotherm model; (e) Temkin isotherm model, (f) Dubinin–Radushkevich (D-R) isotherm model (conditions: pH = natural, CCBC = 0.02 g, t = 30 min, shaking = 100 rpm, temperature = 25 °C).

stant (Lmg^{-1}); K_F = Freundlich constant, $((mg/g)(Lg^{-1})^n)$; n = constant (relates adsorption intensity); R = universal gas constant $(JK^{-1}mol^{-1})$; T = temperature (K); K_T = equilibrium binding constant (Lg^{-1}); b = constant (relates heat of adsorption) $(Jmol^{-1})$; K_E = constant (relates mean adsorption energy E from equation (11)) (mol^2kJ^{-2}); ε_p = polanyi potential $(kJ\text{-}mol^{-1})$ defined by equation (12), (Liu et al., 2019).

$$E = \frac{1}{\sqrt{2K_E}} \tag{11}$$

$$\varepsilon_p = RTln(1 + \frac{1}{C_e}) \tag{12}$$

From Langmuir isotherm, the favorability of adsorption process was calculated based on the constant R_L by using Eq. (13) (Medhat et al., 2021; Malik, 2004)

$$R_L = \frac{1}{1 + K_L C_o} \tag{13}$$

Here, C_o = highest initial dye concentration. The R_L value helps in predicting the favorability of the adsorption process (favorable when R_L is greater than zero but <1) (Medhat et al., 2021). The value of adsorption energy E from D-R isothermal model can be used to predict whether an adsorption process is physisorption ($E < 8kJmol^{-1}$) or chemisorption ($8 < E < 16kJmol^{-1}$) (Bering et al., 1972).

Fig. 10 shows the corresponding plots of Langmuir (Fig. 10a and 10b), Freundlich (Fig. 10c and 10d), Temkin (Fig. 10e) and Dubinin–Radushkevich (Fig. 10f) isotherms. Table 4 lists all the important parameters extrapolated from the fitted plots of isothermal models. Best fitted isothermal model for MB adsorption onto CCBC was determined based on the correlation coefficient (R^2) values of the fitted plots. The Linear fitting of Langmuir isotherm exhibited best fitting (R^2 = 0.9995) which also suggests the occurrence of monolayer adsorption process and when an adsorbed particle enters an active site, no further adsorption is carried out (Langmuir, 1918). The maximum adsorption capacity (Q_{max}) was 20.416mgg^{-1} and the R_L value was 0.01, suggesting a favorable adsorption of MB by CCBC.

The adsorption intensity value greater than unity (n greater than 1) in Freundlich adsorption isotherm model also depicts the favorability of the adsorption process. Temkin isotherm model gave equilibrium binding constant value (K_T) and heat of adsorption (b) of 890.63Lmg^{-1} and 907.49Jmol^{-1} respectively. The energy of adsorption (E = 6.34 kJ/mol) from D-R model suggests the physisorption of MB onto CCBC surface.

4.11. Adsorption kinetics

Kinetic models of adsorption give information regarding the rate of reaction, rate controlling step and mechanism of adsorption (Anastopoulos and Kyzas, 2014). In our adsorptive experiment of CCBC and MB, pseudo first and second order, Elovich and intraparticle diffusion kinetic models were exploited. The linear and non-linear expressions of pseudo first and second order kinetic models are given by the equations (14) - (17) and linear form of Elovich and intraparticle diffusion kinetic model is presented in equation (18) and (19) (Yan et al., 2020).

Table 4 Parameters of isotherm plot fittings for the adsorption of mb by ccbc.

Model	Fitting type	Parameters	values
Langmuir	Linear Non-linear	Q_{max} (mgg^{-1})	**20.42**
		K_L (Lmg^{-1})	13.68
		R_L	0.01
		R^2	**0.9995**
		Q_{max} (mgg^{-1})	19.87
		K_L (Lmg^{-1})	16.84
		R_L	0.007
		R^2	0.97193
Freundlich	Linear Non-linear	K_F (mg$^{1-1/n}$L$^{-1/n}$g^{-1})	18.49
		n	5.39
		R_L	0.006
		R^2	0.9358
		K_F (mg$^{1-1/n}$L$^{-1/n}$g^{-1})	18.07
		n	5.34
		R_L	0.005
		R^2	0.95431
Temkin	Linear	K_T (Lmg^{-1})b (Jmol^{-1})	890.63 907.49
		R^2	0.97473
Dubinin-Radushkevich	Linear	Q_{max} (mgg^{-1})	19.25
		K_E (mol^{2}kJ^{-2})E (kJmol^{-1})	0.012 6.34
		R^2	0.96757

$$ln(q_e - q_t) = lnq_e - k_1t \tag{14}$$

$$q_t = q_e(1 - e^{k_1t}) \tag{15}$$

$$\frac{t}{q_t} = \frac{1}{k_2q_e^2} + \frac{t}{q_e} \tag{16}$$

$$q_t = \frac{k_2q_e^2t}{1 + k_2q_et} \tag{17}$$

$$q_t = \frac{lna_eb_e}{b_e} + \frac{1}{b_e}lnt \tag{18}$$

$$q_t = k_it^{0.5} + C_i \tag{19}$$

Here, q_e = amount adsorbed at equilibrium (mgg^{-1}); q_t = amount adsorbed at time t (mg g^{-1}); k_1 and k_2 = rate constant of pseudo first and second order kinetic model (gmg^{-1}min^{-1}); = initial adsorption rate (mgg^{-1}min^{-1}); b_e = degree of surface coverage (gmg^{-1}); k_i = rate constant of intraparticle diffusion model (mgg^{-1}min$^{-0.5}$) and C_i = constant related to thickness of boundary layer (mgg^{-1}).

Pseudo first order kinetic model makes assumption about the adsorption mechanism which is related to the membrane diffusion theory. According to this theory, the rate of adsorption is related to the variation between the adsorption capacity at equilibrium and quantity of adsorbate with time. In this process, reaction rate depends on the concentration of the adsorbate for a mono adsorbate system and this kinetics is known to be governed by physisorption. Conversely, according to the pseudo second order model, the rate of sorption is reciprocal to the rate of adsorption. It includes membrane diffusion, surface adsorption and particle diffusion where chemical reaction among the
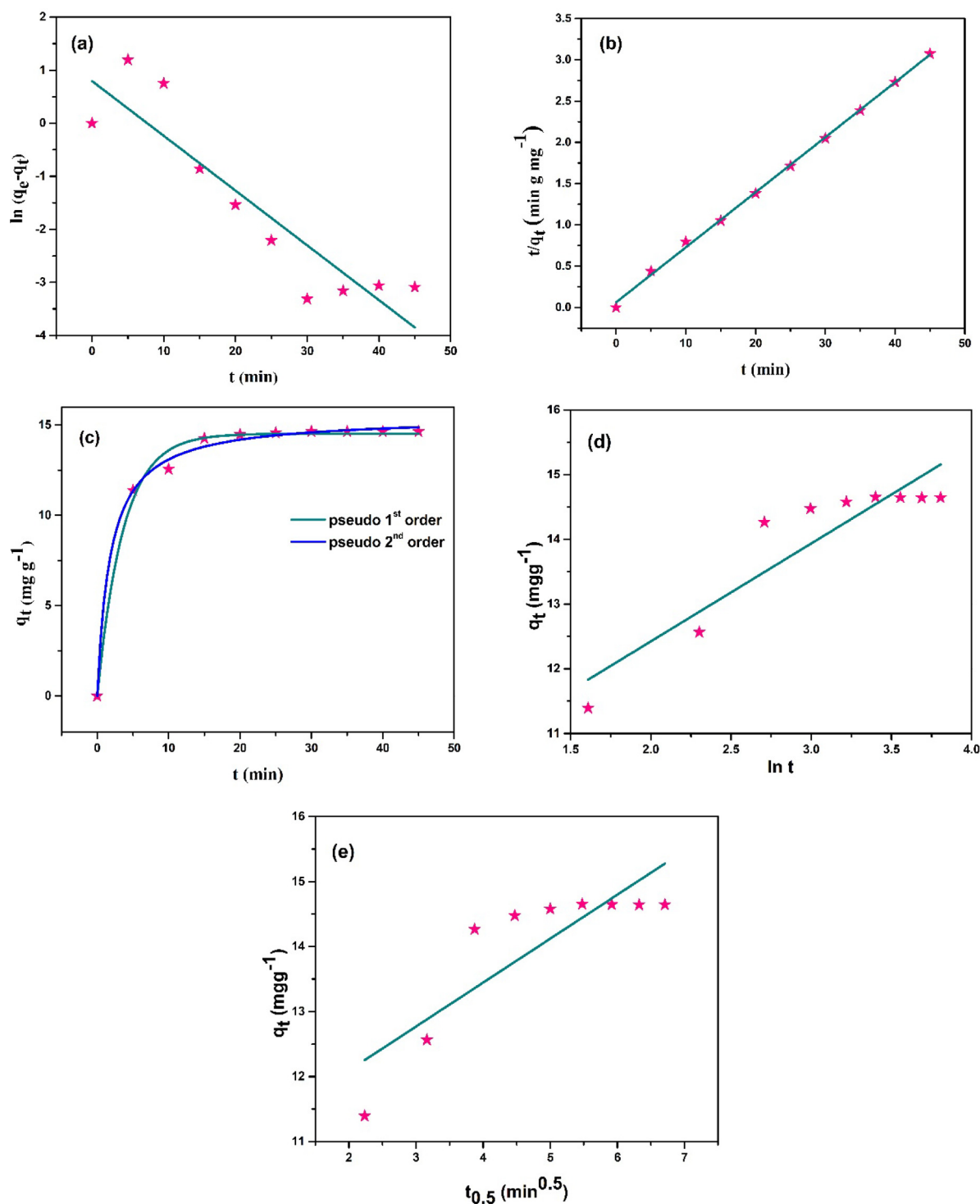
Fig. 11 (a and b) linear and (c) non-linear fitting of pseudo-first and pseudo-second order; (d) Elovich; (e) Intraparticle diffusion kinetic model (Conditions: C_o = 10 ppm, pH = natural, CCBC = 0.02 g, t = 30 min, shaking = 100 rpm, temperature = 25 °C).

adsorbent and the adsorbate is termed as a rate-determining step, hence describe the chemisorption mechanism of the process (Ho and McKay, 1999). Elovich kinetic model was also employed to assist second order kinetics assuming the heterogeneous-based chemisorption process. Mechanism regarding adsorbate-adsorbent interaction is not portrait by this model (Mezenner and Bensmaili, 2009). The intraparticle diffusion model was also exploited for the kinetics calculation. If this

intra-particle diffusion is determined to be the rate controlling step, then a linear plot passing through the origin will be originated. If opposite phenomena occurs, then some extend of boundary layer or other kinetic models might be more appropriate (Arami et al., 2008; Weber Jr and Morris, 1963).

Fig. 11 (a and b) represents the linear fitting of pseudo-first order and pseudo-second order kinetic model whereas Fig. 11 (c) represents their non-linear fitting. The Elovich and Intra-

Table 5 Different kinetic model parameters of MB adsorption by CCBC.

Kinetic model	Curve fitting	Parameters	values
Pseudo-first order	Linear	q_e (mgg^{-1})	2.22
	Non-linear	k_1 (gmg^{-1}min^{-1})	0.103
		R^2	0.8089
		q_e	14.52
		k_1	0.276
		R^2	0.99146
Pseudo-second order	Linear	q_e (mgg^{-1})	15.00
	Non-linear	k_2 (gmg^{-1}min^{-1})	0.071
		R^2	**0.99864**
		q_e (mgg^{-1})	15.48
		k_2 (gmg^{-1}min^{-1})	0.035
		R^2	0.99586
Elovich	Linear	a_e (mgg^{-1}min^{-1})	753.23
		b_e (gmg^{-1})	0.661
		R^2	0.82744
Intraparticle diffusion	Linear	k_1 (mgg^{-1}min$^{-0.5}$)	0.68
		C_i (mgg^{-1})	10.74
		R^2	0.69643

particle diffusion model have been shown in Fig. 11 (d and e) respectively.

The extrapolated values of different parameters from the fitted plots of kinetic models are listed in Table 5. Maximum value of co-relation co-efficient ($R^2 = 0.998$) was obtained from the linear fitting of pseudo second-order kinetic model. The value of C_i in intraparticle diffusion is greater than zero, which means the fitted plot doesn't pass through the origin

and hence intraparticle diffusion is not the rate controlling step (Anastopoulos and Kyzas, 2014).

4.12. Thermodynamics

Gibbs free energy (ΔG_0) can be exploited for approximating the viability of an adsorption process. The spontaneity of a process is depicted by the negative ΔG_0 whereas positive

Table 6 Gibbs free energy calculated using constants from various isotherm models.

isotherm	Fitting	constant	temperature (T), K	Universal gas constant (R), Jmol^{-1}K^{-1}	Gibbs free energy (ΔG_0), KJ/mol
Langmuir	Linear	13.68	298	8.314	−6.48
	Non–linear	16.84			−6.99
Freundlich	Linear	18.49			−7.23
	Non-linear	18.07			−7.17
Temkin	Linear	890.63			−16.83
Dubinin-Radushkevich	Linear	0.012			+ 10.96
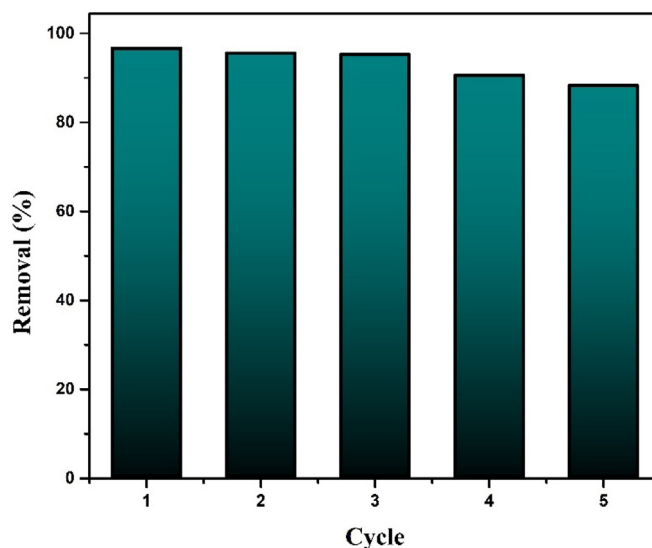
Fig. 12 Regeneration study of CCBC.

ΔG_0 value represents the opposite. Following equation (20) shows the expression of Gibbs free energy (ΔG_0), (Kim et al., 2004).

$$\Delta G_O = -RT \ln(K) \tag{20}$$

Here, T = temperature of the experiment (298 K in all of our experiments), R = universal gas constant (8.314 Jmol^{-1}-K^{-1}) and K = equilibrium constant which has been obtained from Langmuir, Freundlich, Temkin and Dubinin-Radushkevich isotherm models (Nawi et al., 2018). The values obtained are listed in Table 6.

All the values of ΔG_0 are negative except for Dubinin-Radushkevich model which has the value of + 10.96KJ/mol. The negative as well as smaller values of ΔG_0 produced by Langmuir, Freundlich and Temkin models can be termed as indication of feasibility as well as and spontaneity of the adsorption process (Abdulraheem et al., 2015; Yağmur and Kaya, 2021).

4.13. Regeneration and reusability study

Regeneration of used adsorbent is imperative to ensure the economic feasibility as well as to prevent pollution which may occur if this used adsorbent is discharged into environment. In order to perform the desorption study, five adsorption–desorption cycles were carried out with 0.5 M HCl as a regenerating agent.

For this investigation, orbital shaking of 30 ml 10 ppm MB solution was done at 100 rpm for 90 min. The amount of CCBC was 0.02 g. Removal % of MB found to be 96.67% in first cycle, remained almost stable in next two cycle and then fall to 88.28% after the fifth cycle (Fig. 12).

4.14. Adsorption mechanism and comparative study

Biochar is a widely recognized eco-friendly absorbent for removing a wide variety of pollutants because of having a large
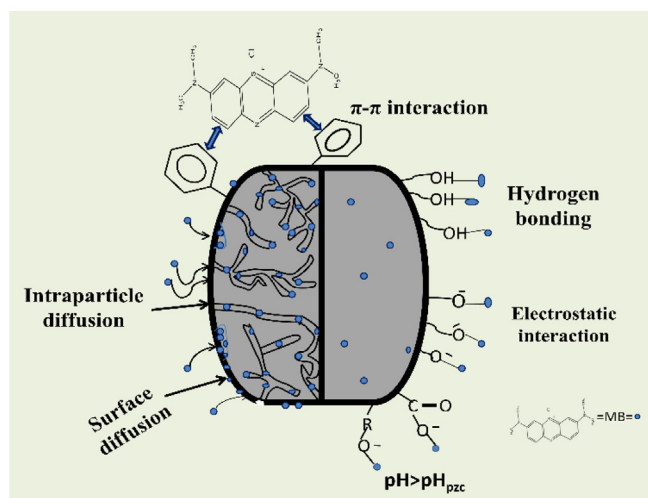

Fig. 13 Mechanism of MB adsorption onto CCBC.

Table 7 Comparison of adsorption efficacy of CCBC prepared from corncob using various techniques.

CCBC preparation technique	Chemical treatment	removed dye	removal % and time	maximum adsorption capacity (mg/g)	Ref.
Pyrolysis at 450–550 °C	sulfuric acid	real textile dye wastewater	98% at 45 min	6.02	(Sonu et al., 2020)
Pyrolysis at 850 °C	potassium hydroxide	MB	99.05% at 180 min	2249	(Yu et al., 2019)
Burning in a chamber at 370–400 °C	–	MB	64% at 15 min	7.58	(Tsamo et al., 2019)
Carbonized at 400 °C	epichlorohydrin mediated composite with chitosan	MB	99.96%	499.8	(Liu et al., 2022)
Hydrothermal carbonization at 160 °C	Phosphoric acid	MB	80% at 120 min	140.25	(Wang et al., 2020)
Pyrolysis at 400 °C	triethylenetetramine	Tartrazine sunset yellow	90.02–90.42% 90.37–92.44%	85.47 74.07	(Mahmoud et al., 2020)
Pyrolysis at 500 °C	–	Brilliant green	91.7 % in 5 days	16.53	(Giri et al., 2020)
Pyrolysis at 700 °C	–	MB	97.72% at 30 min	20.41	This study*

surface area and charged surface (Ambaye et al., 2021). Although the mechanism that governs the adsorption process involves many complex interactions, researchers opine the adsorption process to be comprised of multiple mechanisms, i.e. pore filling, Van Der Waals forces, electrostatic interactions, precipitation and surface sorption, $\pi - \pi$ interactions, cation - π interactions etc. (Srivatsav et al., 2020). Fig. 13 summarizes the possible mechanism that might be governing the adsorptive interaction between MB and CCBC adsorbent.

Table 7 lists a comparison of adsorptive removal of assorted dyes by CCBC prepared through various techniques.

5. Conclusion

A facile preparation technique using in-house built chamber and the potential of CCBC derived from Bangladeshi originated corncob in remediation of MB dye has been studied. Elemental analysis showed variation in wt% of the major elements (C, H, N, O) compared with other regional corncobs. Batch experiment governed the optimum conditions of the adsorption process in terms of dye concentration, adsorbent dose, time interval and pH of the medium. In addition, spontaneity of the process is also confirmed by thermodynamic study. Efficient extermination of MB by CCBC involved a number of mechanisms including surface diffusion, intra-particle diffusion, hydrogen bond interaction, π -π interaction and electrostatic interaction. Therefore, good removal efficacy of MB using CCBC proved that it can be utilized as an adsorbent for eradication of cationic dye from textile waste water.

CRediT authorship contribution statement

Nigar Sultana Pinky: Conceptualization, Methodology, Formal analysis, Investigation, Writing – original draft. **Mashrafi Bin Mobarak:** Writing – original draft, Writing – review & editing, Supervision. **Sonjida Mustafi:** Resources. **Mohammad Zesanur Rahman:** Formal analysis, Investigation. **Aynun Nahar:** Formal analysis, Investigation. **Trissa Saha:** Formal analysis, Investigation. **Newaz Mohammed Bahadur:** Resources.

Declaration of Competing Interest

The authors declare that they have no known competing financial interests or personal relationships that could have appeared to influence the work reported in this paper.

Acknowledgement

References

Abd El-Rahim, W.M., El-Ardy, O.A.M., Mohammad, F.H., 2009. The effect of pH on bioremediation potential for the removal of direct violet textile dye by Aspergillus niger. Desalination 249, 1206–1211.

Abdulraheem, G., Bala, S., Muhammad, S., Abdullahi, M., 2015. Kinetics, equilibrium and thermodynamics studies of CI Reactive Blue 19 dye adsorption on coconut shell based activated carbon. Int. Biodeterior. Biodegrad. 102, 265–273.

Adeogun, A.I., Ofudje, E.A., Idowu, M.A., Kareem, S.O., Vahidhabanu, S., Babu, B.R., 2018. Biowaste-derived hydroxyapatite for effective removal of reactive yellow 4 dye: equilibrium, kinetic, and thermodynamic studies. ACS Omega 3, 1991–2000.

Adesemuyi, M.F., Adebayo, M.A., Akinola, A.O., Olasehinde, E.F., Adewole, K.A., Lajide, L., 2020. Preparation and characterisation of biochars from elephant grass and their utilisation for aqueous nitrate removal: Effect of pyrolysis temperature. J. Environ. Chem. Eng. 8, 104507.

Al-Qodah, Z., Lafi, W.K., Al-Anber, Z., Al-Shannag, M., Harahsheh, A., 2007. Adsorption of methylene blue by acid and heat treated diatomaceous silica. Desalination 217, 212–224.

Ambaye, T.G., Vaccari, M., van Hullebusch, E.D., Amrane, A., Rtimi, S., 2021. Mechanisms and adsorption capacities of biochar for the removal of organic and inorganic pollutants from industrial wastewater. Int. J. Environ. Sci. Technol. 18, 3273–3294.

Anastopoulos, I., Kyzas, G.Z., 2014. Agricultural peels for dye adsorption: a review of recent literature. J. Mol. Liq. 200, 381–389.

Anupam, K., Swaroop, V., Lal, P.S., Bist, V., 2015. Turning Leucaena leucocephala bark to biochar for soil application via statistical modelling and optimization technique. Ecol. Eng. 82, 26–39.

Arami, M., Limaee, N.Y., Mahmoodi, N.M., 2008. Evaluation of the adsorption kinetics and equilibrium for the potential removal of acid dyes using a biosorbent. Chem. Eng. J. 139, 2–10.

Barquilha, C.E., Braga, M.C., 2021. Adsorption of organic and inorganic pollutants onto biochars: challenges, operating conditions, and mechanisms. Bioresour. Technol. Rep. 15, 100728.

Barquilha, C.E.R., Cossich, E.S., Tavares, C.R.G., Silva, E.A., 2019. Biosorption of nickel (II) and copper (II) ions by Sargassum sp. in nature and alginate extraction products. Bioresour. Technol. Rep. 5, 43–50.

Bering, B.P., Dubinin, M.M., Serpinsky, V.V., 1972. On thermodynamics of adsorption in micropores. J. Colloid Interface Sci. 38, 185–194.

Bessy, T.C., Bindhu, M.R., Johnson, J., Chen, S.-M., Chen, T.-W., Almaary, K.S., 2022. UV light assisted photocatalytic degradation of textile waste water by Mg0. 8-xZnxFe2O4 synthesized by combustion method and in-vitro antimicrobial activities. Environ. Res. 204, 111917.

Bhatnagar, A., Sillanpää, M., 2010. Utilization of agro-industrial and municipal waste materials as potential adsorbents for water treatment—a review. Chem. Eng. J. 157, 277–296.

Bonilla-Petriciolet, A., Mendoza-Castillo, D.I., Reynel-Ávila, H.E., 2017. Adsorption processes for water treatment and purification. Springer.

Bridgwater, A.V., 2012. Review of fast pyrolysis of biomass and product upgrading. Biomass Bioenergy 38, 68–94.

Cha, J.S., Park, S.H., Jung, S.-C., Ryu, C., Jeon, J.-K., Shin, M.-C., Park, Y.-K., 2016. Production and utilization of biochar: A review. J. Ind. Eng. Chem. 40, 1–15.

Chakraborty, P., Banerjee, S., Kumar, S., Sadhukhan, S., Halder, G., 2018. Elucidation of ibuprofen uptake capability of raw and steam activated biochar of Aegle marmelos shell: isotherm, kinetics, thermodynamics and cost estimation. Process Saf. Environ. Prot. 118, 10–23.

Chan, S.H.S., Yeong Wu, T., Juan, J.C., Teh, C.Y., 2011. Recent developments of metal oxide semiconductors as photocatalysts in advanced oxidation processes (AOPs) for treatment of dye wastewater. J. Chem. Technol. Biotechnol. 86, 1130–1158.

Chen, Y., Yang, H., Wang, X., Zhang, S., Chen, H., 2012. Biomass-based pyrolytic polygeneration system on cotton stalk pyrolysis: influence of temperature. Bioresour. Technol. 107, 411–418.

Cruz, G.J., Mondal, D., Rimaycuna, J., Soukup, K., Gómez, M.M., Solis, J.L., Lang, J., 2020. Agrowaste derived biochars impregnated with ZnO for removal of arsenic and lead in water. J. Environ. Chem. Eng. 8, 103800.

De Bhowmick, G., Sarmah, A.K., Sen, R., 2019. Zero-waste algal biorefinery for bioenergy and biochar: a green leap towards achieving energy and environmental sustainability. Sci. Total Environ. 650, 2467–2482.

Demiral, I., Eryazıcı, A., Şensöz, S., 2012. Bio-oil production from pyrolysis of corncob (Zea mays L.). Biomass Bioenergy 36, 43–49.

Demirbas, A., 2004. Effects of temperature and particle size on biochar yield from pyrolysis of agricultural residues. J. Anal. Appl. Pyrolysis 72, 243–248.

Dieguez-Alonso, A., Funke, A., Anca-Couce, A., Rombolà, A.G., Ojeda, G., Bachmann, J., Behrendt, F., 2018. Towards biochar and hydrochar engineering—Influence of process conditions on surface physical and chemical properties, thermal stability, nutrient availability, toxicity and wettability. Energies 11, 496.

Dotto, G.L., McKay, G., 2020. Current scenario and challenges in adsorption for water treatment. J. Environ. Chem. Eng. 8, 103988.

Dubinin, M.M., 1947. The equation of the characteristic curve of activated charcoal, in: Dokl. Akad. Nauk. SSSR. pp. 327–329.

El Haddad, M., Mamouni, R., Saffaj, N., Lazar, S., 2012. Removal of a cationic dye–Basic Red 12–from aqueous solution by adsorption onto animal bone meal. J. Assoc. Arab Univ. Basic Appl. Sci. 12, 48–54.

Foo, K.Y., Hameed, B.H., 2011. The environmental applications of activated carbon/zeolite composite materials. Adv. Colloid Interface Sci. 162, 22–28.

Freundlich, H.M.F., 1906. Over the adsorption in solution. J. Phys. Chem. 57, 1100–1107.

Ganguly, P., Sarkhel, R., Das, P., 2020. Synthesis of pyrolyzed biochar and its application for dye removal: Batch, kinetic and isotherm with linear and non-linear mathematical analysis. Surf. Interfaces 20, 100616.

Gatabi, M.P., Moghaddam, H.M., Ghorbani, M., 2016. Point of zero charge of maghemite decorated multiwalled carbon nanotubes fabricated by chemical precipitation method. J. Mol. Liq. 216, 117–125.

Gayathri, R., Gopinath, K.P., Kumar, P.S., 2021. Adsorptive separation of toxic metals from aquatic environment using agro waste biochar: application in electroplating industrial wastewater. Chemosphere 262, 128031.

Ghodke, P.K., Sharma, A.K., Pandey, J.K., Chen, W.-H., Patel, A., Ashokkumar, V., 2021. Pyrolysis of sewage sludge for sustainable biofuels and value-added biochar production. J. Environ. Manage. 298, 113450.

Giri, B.S., Gun, S., Pandey, S., Trivedi, A., Kapoor, R.T., Singh, R. P., Abdeldayem, O.M., Rene, E.R., Yadav, S., Chaturvedi, P., 2020. Reusability of brilliant green dye contaminated wastewater using corncob biochar and Brevibacillus parabrevis: hybrid treatment and kinetic studies. Bioengineered 11, 743–758.

Gonzalez-Canche, N.G., Carrillo, J.G., Escobar-Morales, B., Salgado-Tránsito, I., Pacheco, N., Pech-Cohuo, S.C., Peña-Cruz, M. I., 2021. Physicochemical and optical characterization of citrus aurantium derived biochar for solar absorber applications. Materials 14, 4756.

Gupta, V.K., Carrott, P.J.M., Ribeiro Carrott, M.M.L., Suhas, 2009. Low-cost adsorbents: growing approach to wastewater treatment—a review. Crit. Rev. Environ. Sci. Technol. 39, 783–842.

Gupta, G.K., Ram, M., Bala, R., Kapur, M., Mondal, M.K., 2018. Pyrolysis of chemically treated corncob for biochar production and its application in Cr (VI) removal. Environ. Prog. Sustain. Energy 37, 1606–1617.

Hao, F., Zhao, X., Ouyang, W., Lin, C., Chen, S., Shan, Y., Lai, X., 2013. Molecular structure of corncob-derived biochars and the mechanism of atrazine sorption. Agron. J. 105, 773–782.

Hasan, E., Tarhule, A., Hong, Y., Moore III, B., 2019. Assessment of physical water scarcity in Africa using GRACE and TRMM satellite data. Remote Sens. 11, 904.

Helfferich, F.G., 1985. Principles of adsorption & adsorption processes, by DM Ruthven, John Wiley & Sons, 1984, xxiv+ 433 pp.

Hemavathy, R.V., Kumar, P.S., Kanmani, K., Jahnavi, N., 2020. Adsorptive separation of Cu (II) ions from aqueous medium using thermally/chemically treated Cassia fistula based biochar. J. Clean. Prod. 249, 119390.

Ho, Y.-S., McKay, G., 1999. Pseudo-second order model for sorption processes. Process Biochem. 34, 451–465.

Hossain, N., Nizamuddin, S., Griffin, G., Selvakannan, P., Mubarak, N.M., Mahlia, T.M.I., 2020. Synthesis and characterization of rice husk biochar via hydrothermal carbonization for wastewater treatment and biofuel production. Sci. Rep. 10, 1–15.

Inyang, M.I., Gao, B., Yao, Y., Xue, Y., Zimmerman, A., Mosa, A., Pullammanappallil, P., Ok, Y.S., Cao, X., 2016. A review of biochar as a low-cost adsorbent for aqueous heavy metal removal. Crit. Rev. Environ. Sci. Technol. 46, 406–433.

Issaka, E., Fapohunda, F.O., Amu-Darko, J.N.O., Yeboah, L., Yakubu, S., Varjani, S., Ali, N., Bilal, M., 2022. Biochar-based composites for remediation of polluted wastewater and soil environments: Challenges and prospects. Chemosphere 297, 134163.

Jothirani, R., Kumar, P.S., Saravanan, A., Narayan, A.S., Dutta, A., 2016. Ultrasonic modified corn pith for the sequestration of dye from aqueous solution. J. Ind. Eng. Chem. 39, 162–175.

Keskin, B., Ersahin, M.E., Ozgun, H., Koyuncu, I., 2021. Pilot and full-scale applications of membrane processes for textile wastewater treatment: A critical review. J. Water Process Eng. 42, 102172.

Kim, Y., Kim, C., Choi, I., Rengaraj, S., Yi, J., 2004. Arsenic removal using mesoporous alumina prepared via a templating method. Environ. Sci. Technol. 38, 924–931.

Kloss, S., Zehetner, F., Dellantonio, A., Hamid, R., Ottner, F., Liedtke, V., Schwanninger, M., Gerzabek, M.H., Soja, G., 2012. Characterization of slow pyrolysis biochars: effects of feedstocks and pyrolysis temperature on biochar properties. J. Environ. Qual. 41, 990–1000.

Kong, S.-H., Loh, S.-K., Bachmann, R.T., Rahim, S.A., Salimon, J., 2014. Biochar from oil palm biomass: A review of its potential and challenges. Renew. Sustain. Energy Rev. 39, 729–739.

Kumar, P.S., Ramalingam, S., Abhinaya, R.V., Thiruvengadaravi, K.V., Baskaralingam, P., Sivanesan, S., 2011. Lead (II) adsorption onto sulphuric acid treated cashew nut shell. Sep. Sci. Technol. 46, 2436–2449.

Kumar, P.S., Gayathri, R., Rathi, B.S., 2021. A review on adsorptive separation of toxic metals from aquatic system using biochar produced from agro-waste. Chemosphere 285, 131438.

Kumar, N.S., Shaikh, H.M., Asif, M., Al-Ghurabi, E.H., 2021. Engineered biochar from wood apple shell waste for high-efficient removal of toxic phenolic compounds in wastewater. Sci. Rep. 11, 1–17.

Kwapinski, W., Byrne, C.M., Kryachko, E., Wolfram, P., Adley, C., Leahy, J.J., Novotny, E.H., Hayes, M.H., 2010. Biochar from biomass and waste. Waste Biomass Valorization 1, 177–189.

Kyzas, G.Z., Matis, K.A., 2015. Nanoadsorbents for pollutants removal: a review. J. Mol. Liq. 203, 159–168.

Langmuir, I., 1918. The adsorption of gases on plane surfaces of glass, mica and platinum. J. Am. Chem. Soc. 40, 1361–1403.

Liu, L., Luo, X.-B., Ding, L., Luo, S.-L., 2019. Application of nanotechnology in the removal of heavy metal from water, in: Nanomaterials for the Removal of Pollutants and Resource Reutilization. Elsevier, pp. 83–147.

Liu, X.-J., Li, M.-F., Ma, J.-F., Bian, J., Peng, F., 2022. Chitosan crosslinked composite based on corncob lignin biochar to adsorb methylene blue: Kinetics, isotherm, and thermodynamics. Colloids Surf. Physicochem. Eng. Asp. 642, 128621.

Liu, X., Zhang, Y., Li, Z., Feng, R., Zhang, Y., 2014. Characterization of corncob-derived biochar and pyrolysis kinetics in comparison with corn stalk and sawdust. Bioresour. Technol. 170, 76–82.

Lonappan, L., Rouissi, T., Das, R.K., Brar, S.K., Ramirez, A.A., Verma, M., Surampalli, R.Y., Valero, J.R., 2016. Adsorption of methylene blue on biochar microparticles derived from different waste materials. Waste Manag. 49, 537–544.

Ma, Y., Qi, Y., Yang, L., Wu, L., Li, P., Gao, F., Qi, X., Zhang, Z., 2021. Adsorptive removal of imidacloprid by potassium hydroxide activated magnetic sugarcane bagasse biochar: Adsorption efficiency, mechanism and regeneration. J. Clean. Prod. 292, 126005.

Mahmoud, M.E., Abdelfattah, A.M., Tharwat, R.M., Nabil, G.M., 2020. Adsorption of negatively charged food tartrazine and sunset yellow dyes onto positively charged triethylenetetramine biochar: Optimization, kinetics and thermodynamic study. J. Mol. Liq. 318, 114297.

Maziarka, P., Wurzer, C., Arauzo, P.J., Dieguez-Alonso, A., Mašek, O., Ronsse, F., 2021. Do you BET on routine? The reliability of N2 physisorption for the quantitative assessment of biochar's surface area. Chem. Eng. J. 418, 129234.

Medhat, A., El-Maghrabi, H.H., Abdelghany, A., Menem, N.M.A., Raynaud, P., Moustafa, Y.M., Elsayed, M.A., Nada, A.A., 2021. Efficiently activated carbons from corn cob for methylene blue adsorption. Appl. Surf. Sci. Adv. 3, 100037.

Mezenner, N.Y., Bensmaili, A., 2009. Kinetics and thermodynamic study of phosphate adsorption on iron hydroxide-eggshell waste. Chem. Eng. J. 147, 87–96.

Mishra, A.K., Arockiadoss, T., Ramaprabhu, S., 2010. Study of removal of azo dye by functionalized multi walled carbon nanotubes. Chem. Eng. J. 162, 1026–1034.

Mobarak, M.B., Hossain, M.S., Yeasmin, Z., Mahmud, M., Rahman, M.M., Sultana, S., Masum, S.M., Ahmed, S., 2022. Probing the photocatalytic competency of hydroxyapatite synthesized by solid state and wet chemical precipitation method. J. Mol. Struct. 1252, 132142.

Mohamed Noor, N., Shariff, A., Abdullah, N., 2012. Slow pyrolysis of cassava wastes for biochar production and characterization. Iran. Iran. J. Energy Environ. 3.

Mohan, D., Abhishek, K., Sarswat, A., Patel, M., Singh, P., Pittman, C.U., 2018. Biochar production and applications in soil fertility and carbon sequestration–a sustainable solution to crop-residue burning in India. RSC Adv. 8, 508–520.

Moosavi, S., Lai, C.W., Gan, S., Zamiri, G., Akbarzadeh Pivehzhani, O., Johan, M.R., 2020. Application of efficient magnetic particles and activated carbon for dye removal from wastewater. ACS Omega 5, 20684–20697.

Mullen, C.A., Boateng, A.A., Goldberg, N.M., Lima, I.M., Laird, D.A., Hicks, K.B., 2010. Bio-oil and bio-char production from corn cobs and stover by fast pyrolysis. Biomass Bioenergy 34, 67–74.

Nanda, S., Dalai, A.K., Berruti, F., Kozinski, J.A., 2016. Biochar as an exceptional bioresource for energy, agronomy, carbon sequestration, activated carbon and specialty materials. Waste Biomass Valorization 7, 201–235.

Nath, H., Saikia, A., Goutam, P.J., Saikia, B.K., Saikia, N., 2021. Removal of methylene blue from water using okra (Abelmoschus esculentus L.) mucilage modified biochar. Bioresour. Technol. Rep. 14, 100689.

Nawi, M.A., Sabar, S., Nawawi, W.I., 2018. Preparation of immobilized activated carbon-polyvinyl alcohol composite for the adsorptive removal of 2, 4-dichlorophenoxyacetic acid. J. Water Process Eng. 25, 269–277.

Ng, W.C., You, S., Ling, R., Gin, K.-Y.-H., Dai, Y., Wang, C.-H., 2017. Co-gasification of woody biomass and chicken manure: Syngas production, biochar reutilization, and cost-benefit analysis. Energy 139, 732–742.

Oluk, I., Nagawa, C.B., Banadda, N., Tumutegyereize, P., Owusu, P.A., 2021. Development of maize cob-based biochar filter for water purification. Water Environ. J. 35, 349–358.

Ong, Y.K., Li, F.Y., Sun, S.-P., Zhao, B.-W., Liang, C.-Z., Chung, T.-S., 2014. Nanofiltration hollow fiber membranes for textile wastewater treatment: Lab-scale and pilot-scale studies. Chem. Eng. Sci. 114, 51–57.

Padmavathy, K.S., Madhu, G., Haseena, P.V., 2016. A study on effects of pH, adsorbent dosage, time, initial concentration and adsorption isotherm study for the removal of hexavalent chromium (Cr (VI)) from wastewater by magnetite nanoparticles. Procedia Technol. 24, 585–594.

Palansooriya, K.N., Yang, Y., Tsang, Y.F., Sarkar, B., Hou, D., Cao, X., Meers, E., Rinklebe, J., Kim, K.-H., Ok, Y.S., 2020. Occurrence of contaminants in drinking water sources and the potential of biochar for water quality improvement: A review. Crit. Rev. Environ. Sci. Technol. 50, 549–611.

Petronijević, M., Panić, S., Savić, S., Agbaba, J., Jazić, J.M., Milanović, M., \DJurišić-Mladenović, N., 2021. Characterization and application of biochar-immobilized crude horseradish peroxidase for removal of phenol from water. Colloids Surf. B Biointerfaces 208, 112038.

Pohanish, R.P., 2017. Sittig's handbook of toxic and hazardous chemicals and carcinogens. William Andrew.

Quispe, J.B., Campos, L.C., Mašek, O., Bogush, A., 2022. Use of biochar-based column filtration systems for greywater treatment: A systematic literature review. J. Water Process Eng. 48, 102908.

Rafiq, M.K., Bachmann, R.T., Rafiq, M.T., Shang, Z., Joseph, S., Long, R., 2016. Influence of pyrolysis temperature on physico-chemical properties of corn stover (Zea mays L.) biochar and feasibility for carbon capture and energy balance. PloS One 11, e0156894.

Ro, K.S., Cantrell, K.B., Hunt, P.G., 2010. High-temperature pyrolysis of blended animal manures for producing renewable energy and value-added biochar. Ind. Eng. Chem. Res. 49, 10125–10131.

Saini, A., Maheshwari, P.H., Tripathy, S.S., Waseem, S., Dhakate, S.R., 2020. Processing of rice straw to derive carbon with efficient de-fluoridation properties for drinking water treatment. J. Water Process Eng. 34, 101136.

Saremi, F., Miroliaei, M.R., Nejad, M.S., Sheibani, H., 2020. Adsorption of tetracycline antibiotic from aqueous solutions onto vitamin B6-upgraded biochar derived from date palm leaves. J. Mol. Liq. 318, 114126.

Shahmirzadi, M.A.A., Kargari, A., 2018. Nanocomposite membranes, in: Emerging Technologies for Sustainable Desalination Handbook. Elsevier, pp. 285–330.

Shakoor, M.B., Ali, S., Rizwan, M., Abbas, F., Bibi, I., Riaz, M., Khalil, U., Niazi, N.K., Rinklebe, J., 2020. A review of biochar-based sorbents for separation of heavy metals from water. Int. J. Phytoremed. 22, 111–126.

Shirmardi, M., Alavi, N., Lima, E.C., Takdastan, A., Mahvi, A.H., Babaei, A.A., 2016. Removal of atrazine as an organic micro-pollutant from aqueous solutions: a comparative study. Process Saf. Environ. Prot. 103, 23–35.

Sobhani, A., 2022. Hydrothermal synthesis of CuMn2O4/CuO nanocomposite without capping agent and study its photocatalytic activity for elimination of dye pollution. Int. J. Hydrog. Energy.

Sohi, S., Lopez-Capel, E., Krull, E., Bol, R., 2009. Biochar, climate change and soil: A review to guide future research. CSIRO Land Water Sci. Rep. 5, 17–31.

Sonu, K., Sogani, M., Syed, Z., Dongre, A., Sharma, G., 2020. Enhanced decolorization and treatment of textile dye wastewater through adsorption on acid modified corncob derived biochar. ChemistrySelect 5, 12287–12297.

Spokas, K.A., 2010. Review of the stability of biochar in soils: predictability of O: C molar ratios. Carbon Manag. 1, 289–303.

Srivatsav, P., Bhargav, B.S., Shanmugasundaram, V., Arun, J., Gopinath, K.P., Bhatnagar, A., 2020. Biochar as an eco-friendly and economical adsorbent for the removal of colorants (dyes) from aqueous environment: A review. Water 12, 3561.

Stefaniuk, M., Oleszczuk, P., 2015. Characterization of biochars produced from residues from biogas production. J. Anal. Appl. Pyrolysis 115, 157–165.

Subratti, A., Vidal, J.L., Lalgee, L.J., Kerton, F.M., Jalsa, N.K., 2021. Preparation and characterization of biochar derived from the fruit seed of Cedrela odorata L and evaluation of its adsorption capacity with methylene blue. Sustain. Chem. Pharm. 21, 100421.

Suganya, S., Saravanan, A., Ravikumar, C., 2017. Computation of adsorption parameters for the removal of dye from wastewater by microwave assisted sawdust: theoretical and experimental analysis. Environ. Toxicol. Pharmacol. 50, 45–57.

Sumalinog, D.A.G., Capareda, S.C., de Luna, M.D.G., 2018. Evaluation of the effectiveness and mechanisms of acetaminophen and methylene blue dye adsorption on activated biochar derived from municipal solid wastes. J. Environ. Manage. 210, 255–262.

Suwunwong, T., Hussain, N., Chantrapromma, S., Phoungthong, K., 2020. Facile synthesis of corncob biochar via in-house modified pyrolysis for removal of methylene blue in wastewater. Mater. Res. Express 7, 015518.

Tavangar, T., Jalali, K., Shahmirzadi, M.A.A., Karimi, M., 2019. Toward real textile wastewater treatment: Membrane fouling control and effective fractionation of dyes/inorganic salts using a hybrid electrocoagulation–Nanofiltration process. Sep. Purif. Technol. 216, 115–125.

Temkin, M.I., 1940. Kinetics of ammonia synthesis on promoted iron catalysts. Acta Physiochim. URSS 12, 327–356.

Tian, Y., Zhang, J., Zuo, W., Chen, L., Cui, Y., Tan, T., 2013. Nitrogen conversion in relation to NH3 and HCN during microwave pyrolysis of sewage sludge. Environ. Sci. Technol. 47, 3498–3505.

Trninić, M., Wang, L., Várhegyi, G., Grønli, M., Skreiberg, Ø., 2012. Kinetics of corncob pyrolysis. Energy Fuels 26, 2005–2013.

Tsamo, C., Assabe, M., Argue, J., Ihimbru, S.O., 2019. Discoloration of methylene blue and slaughter house wastewater using maize cob biochar produced using a constructed burning chamber: a comparative study. Sci. Afr. 3, e00078.

Varsha, M., Kumar, P.S., Rathi, B.S., 2022. A review on recent trends in the removal of emerging contaminants from aquatic environment using low-cost adsorbents. Chemosphere 287, 132270.

Villagómez-Salas, S., Manikandan, P., Acuna Guzman, S.F., Pol, V. G., 2018. Amorphous carbon chips li-ion battery anodes produced through polyethylene waste upcycling. ACS Omega 3, 17520–17527.

Vyavahare, G., Gurav, R., Patil, R., Sutar, S., Jadhav, P., Patil, D., Yang, Y.-H., Tang, J., Chavan, C., Kale, S., 2021. Sorption of brilliant green dye using soybean straw-derived biochar: characterization, kinetics, thermodynamics and toxicity studies. Environ. Geochem. Health 43, 2913–2926.

Wang, W., Gong, Q., Chen, Z., Wang, W.D., Huang, Q., Song, S., Chen, J., Wang, X., 2019. Adsorption and competition investigation of phenolic compounds on the solid-liquid interface of three-dimensional foam-like graphene oxide. Chem. Eng. J. 378, 122085.

Wang, X., Jiang, C., Hou, B., Wang, Y., Hao, C., Wu, J., 2018. Carbon composite lignin-based adsorbents for the adsorption of dyes. Chemosphere 206, 587–596.

Wang, P., Tyndall, S., Rahman, T., Roy, P., Jahromi, H., Adhikari, S., Boersma, M., 2022. Sorption and recovery of phenolic compounds from aqueous phase of sewage sludge hydrothermal liquefaction using bio-char. Chemosphere 287, 131934.

Wang, X., Xu, J., Sun, T., Ali, S., 2021. Synthesis of Cordyceps fumosorosea-biochar nanoparticles and their effects on growth and survival of Bemisia tabaci (Gennadius). Front. Microbiol. 12, 630220.

Wang, Y., Zhou, Y., Jiang, G., Chen, P., Chen, Z., 2020. One-step fabrication of carbonaceous adsorbent from corncob for enhancing adsorption capability of methylene blue removal. Sci. Rep. 10, 1–9.

Weber Jr, W.J., Morris, J.C., 1963. Kinetics of adsorption on carbon from solution. J. Sanit. Eng. Div. 89, 31–59.

Worasuwannarak, N., Sonobe, T., Tanthapanichakoon, W., 2007. Pyrolysis behaviors of rice straw, rice husk, and corncob by TG-MS technique. J. Anal. Appl. Pyrolysis 78, 265–271.

Wu, J., Yang, J., Feng, P., Huang, G., Xu, C., Lin, B., 2020. High-efficiency removal of dyes from wastewater by fully recycling litchi peel biochar. Chemosphere 246, 125734.

Yaashikaa, P.R., Kumar, P.S., Varjani, S., Saravanan, A., 2020. A critical review on the biochar production techniques, characterization, stability and applications for circular bioeconomy. Biotechnol. Rep. 28, e00570.

Yağmur, H.K., Kaya, İ., 2021. Synthesis and characterization of magnetic ZnCl2-activated carbon produced from coconut shell for the adsorption of methylene blue. J. Mol. Struct. 1232, 130071.

Yan, L., Liu, Y., Zhang, Y., Liu, S., Wang, C., Chen, W., Liu, C., Chen, Z., Zhang, Y., 2020. ZnCl2 modified biochar derived from aerobic granular sludge for developed microporosity and enhanced adsorption to tetracycline. Bioresour. Technol. 297, 122381.

Yang, J., Yu, M., Chen, W., 2015. Adsorption of hexavalent chromium from aqueous solution by activated carbon prepared from longan seed: Kinetics, equilibrium and thermodynamics. J. Ind. Eng. Chem. 21, 414–422.

Yaseen, Z.M., Zigale, T.T., Salih, S.Q., Awasthi, S., Tung, T.M., Al-Ansari, N., Bhagat, S.K., 2019. Laundry wastewater treatment using a combination of sand filter, bio-char and teff straw media. Sci. Rep. 9, 1–11.

Yeboah, M.L., Li, X., Zhou, S., 2020. Facile fabrication of biochar from palm kernel shell waste and its novel application to magnesium-based materials for hydrogen storage. Materials 13, 625.

Yu, Y., Wan, Y., Shang, H., Wang, B., Zhang, P., Feng, Y., 2019. Corncob-to-xylose residue (CCXR) derived porous biochar as an excellent adsorbent to remove organic dyes from wastewater. Surf. Interface Anal. 51, 234–245.

Zhang, Y., Fan, R., Zhang, Q., Chen, Y., Sharifi, O., Leszczynska, D., Zhang, R., Dai, Q., 2019. Synthesis of CaWO4-biochar nanocomposites for organic dye removal. Mater. Res. Bull. 110, 169–173.

Zhao, J., Gao, F., Sun, Y., Fang, W., Li, X., Dai, Y., 2021. New use for biochar derived from bovine manure for tetracycline removal. J. Environ. Chem. Eng. 9, 105585.

Zhao, S.-X., Ta, N., Wang, X.-D., 2017. Effect of temperature on the structural and physicochemical properties of biochar with apple tree branches as feedstock material. Energies 10, 1293.

Zhu, Y., Yi, B., Yuan, Q., Wu, Y., Wang, M., Yan, S., 2018. Removal of methylene blue from aqueous solution by cattle manure-derived low temperature biochar. RSC Adv. 8, 19917–19929.

P.K. Malik, Dye removal from wastewater using activated carbon developed from sawdust: adsorption equilibrium and kinetics, Journal of Hazardous Materials, Volume 113, Issues 1–3, 2004, Pages 81-88, ISSN 0304-3894,